Theory of the photopyroelectric method for investigation of optical and thermal materials properties

M. Chirtoc and G. Mihăilescu
Institute for Isotopic and Molecular Technology, P.O. Box 700, R-3400 Cluj-Napoca 5, Romania
(Received 21 February 1989; revised manuscript received 30 May 1989)

The photopyroelectric (PPE) method is a spectroscopic- and thermal-property investigation technique based on a photothermal effect, consisting of the heating of a sample via nonradiative deexcitation processes following absorption of radiation. The resulting temperature increase is measured by a pyroelectric transducer placed in thermal contact with the sample. The theory for a periodically modulated excitation is developed, assuming a one-dimensional heat-flow process in a model cell composed of six layers and having a finite reflectance at the interface between the sample and the pyroelectric material. Special effort was devoted to the exhaustive analytic and numeric analysis of the general expression for the PPE signal and its special cases, as a function of dimensionless thermal and optical parameters of the sample. The great diversity of the typical response types is shown to originate in the interplay between saturation, optical absorption, and optical or thermal transmission effects. The usefulness of the theory relies on its ability to predict and to interpret the results which can be obtained in a large variety of PPE experimental configurations.

I. INTRODUCTION

In recent years there has been an increasing interest in a group of optically excited thermal processes, known as photothermal effects, which benefit from the use of lasers as precisely controlled heat sources. The derived applications made available new and convenient methods to investigate thermal properties and optical absorption in matter, deexcitation mechanisms and very well spatially and temporally localized, thermally related processes. The photothermal effects are generated by deposition of heat in a sample following absorption of energetic beams via either a direct heating channel provided by thermal deexcitations, or other competing nonthermal deexcitation channels like photoelectric, photochemical, luminescence, and energy-transfer processes which may result, in the end, in indirect heating of the sample.[1]

If the excitation is modulated, the corresponding time- and space-dependent temperature profile developed in the sample gives rise to a variety of different effects such as direct or indirect photoacoustic-wave generation, refractive-index gradients, surface deformation, changes of infrared spectral features and, most directly, to temperature increase of the sample, each of them constituting the basis for a distinct experimental technique, i.e., photoacoustic spectroscopy, photothermal deflection and displacement spectroscopy, photothermal radiometry, and optical calorimetry, respectively.[1-4] The temperature-rise monitoring is less sophisticated, but with sensors like thermocouples or thermistors[5-11] the method is slow, relatively insensitive, and subjected to an ambient-temperature drift.

It is surprising that the sensitivity and the unique intrinsic capability of thermal sensors based on the pyroelectric effect to respond very rapidly, in the subnanosecond range, to thermal excitations have not been exploited in conjunction with photothermal phenomena until recently, despite the impressive theoretical and experimental amount of work devoted to the applications of the pyroelectric effect.[12,13] The possibility of pyroelectric detection of radiation was put forward in 1938 (Ref. 14) and demonstrated experimentally in 1962.[15] In 1965 a temperature-measurement resolution of 10^{-6} K was achieved.[16] It was the joint use of both these sensitive methods, i.e., the radiation and temperature-measurement capabilities, that marked in 1984 the appearance of a new spectroscopic technique for solids,[17-19] designated as photopyroelectric (PPE) spectroscopy.[18] A theory describing it was soon developed for the case of periodic excitation.[20]

The PPE technique consists of the measurement of the temperature increase of a sample due to the absorption of radiation, by placing a pyroelectric transducer in thermal contact with the sample. From the perspective of this definition some earlier papers dealing with systems composed of pyroelectric sensors in thermal contact with absorbing layers and substrates may be regarded also as PPE experiments.[21-25] However, no report contained explicitly the aim to obtain in this way spectroscopic information on a material. Both in PPE experiments and in pyroelectric radiometry one needs essentially a radiation source and a sensor composed of a pyroelectric element and an absorber. It follows that the PPE technique has appeared not in conjunction with the development of a new device but rather with the shift of interest from the radiation source to the absorbing material, in the same experimental configuration. Hence, the present theory can be applied in a straightforward manner to pyroelectric radiation detectors as well, thus unifying different formalisms for their thermal analysis, e.g., Refs. 21, 22, and 26–29.

The calorimetric techniques and especially the PPE

one are the only photothermal techniques based on the direct detection of photothermal heating, i.e., on the temperature change, and therefore it has a number of advantages over other detection schemes involving secondary mechanisms,[30,31] since each conversion step in the signal-generation chain degrades the overall signal-to-noise ratio, sensitivity and bandwidth performance and complicates the theoretical interpretation of the results. A PPE experiment is rather simple to design and usually the specimen needs no preparation, although quantitative determinations require some calibration procedures. The materials that can be investigated range from weakly absorbing solids like thin films[17,32–34] or liquids,[35] semiconductors,[36] surfaces, and adsorbates,[30,33,37,38] to strongly absorbing solids[19] and liquids,[39,40] or diffusing materials.[18] The obtained spectra are comparable to those obtained using pure optical methods if the nonradiative quantum efficiency reaches unity or is at least wavelength independent. Alternatively, by comparing two such spectra, intermolecular energy-transfer processes and nonradiative quantum efficiencies can be studied.[30,32,41,42] Due to the fact that the PPE signal depends on the optical properties and also on the thermal properties of the sample, nonspectroscopic problems can be addressed too, such as thermal microscopy,[43,44] depth profiling,[32,45] investigation of multilayered structures[46,47] and anisotropic media,[48] reaction kinetics,[18] thermal diffusivity measurements,[23,24,49–54] and phase transitions in solids monitored during laser annealing[55] or via temperature dependence of the specific heat.[56] Several approaches are possible in which the excitation and detection is harmonic, pulsed, or modulated in a wide bandwidth,[57] each having specific advantages and drawbacks.[58]

The earlier theory of the PPE technique with periodic excitation[20] assumed total absorption of the radiation by the pyroelectric sensor. The starting point of the present theory was the goal to mark a further step in understanding the role played by a finite reflectance at the sample-pyroelectric interface and the mechanisms responsible for the peak inversions observed in the reflection-mode PPE spectroscopy,[40,59] since these questions have found no satisfactory answers in the framework of the former theory.

II. THE GENERAL PHOTOPYROELECTRIC RESPONSE

In PPE experiments the radiation-receiving area of the cell is typically much larger than the thickness of the sandwiched layers, so that a one-dimensional analysis is fully justified. In Fig. 1 is shown the layout of a PPE cell design that fits most experimental geometries reported for solids or liquids and eventually for gases, by allowing certain layer thicknesses L_i, $i=g,w,m,p,s,b$, to tend to infinity or to zero. The cell is irradiated uniformly by a monochromatic light with wavelength λ and irradiance H_0 ($\mathrm{W\,m^{-2}}$) modulated with a chopper at an angular frequency ω. It is assumed that the thermally thin metallic front electrode is opaque but, acting as a reflector with reflectance $R(\lambda)$, it absorbs only a fraction $1-R$ of the

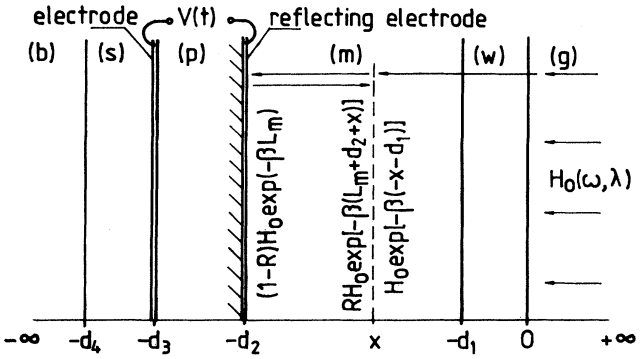

FIG. 1. The one-dimensional geometry of a reflection-mode PPE cell. The irradiation components giving rise to heat sources in the reflector and at an arbitrary depth x in the sample are also shown: g, gas; w, window; m, material specimen; p, pyroelectric; s, substrate; b, backing material.

radiation impinging on it, the rest being reflected back into the material specimen having the bulk absorption coefficient $\beta(\lambda)$. Other reflections at interfaces and interference phenomena are neglected, so that the consideration of the heat sources in terms of the optical properties of a multilayer system[60] is unnecessary. The fast radiationless deexcitations following the absorption upon the double path of the radiation lead to local generation of heat within the reflector and the sample, with conversion quantum efficiencies η_r and η_m, respectively. The heat wave propagating from the sample to the adjacent layers produces a periodic temperature field $T_p(x,t)=T_p(x)\exp(i\omega t)$ in the pyroelectric, where it is converted into an electrical signal via the pyroelectric effect. Any pyroelectric material is also piezoelectric and a photoacoustic signal is to be expected too, but there are several possibilities to distinguish between the two effects.[31]

Considering the sensor's equivalent resistance-capacitance (RC) circuit in parallel with the current source $i_s=pA_s d\langle T_p(x,t)\rangle/dt$, the pyroelectric output voltage is given by

$$V(t)=\frac{i\omega\tau_E pL_p}{\epsilon(1+i\omega\tau_E)}\langle T_p(x)\rangle\exp(i\omega t)\ , \tag{2.1}$$

where $\langle T_p(x)\rangle$ is the spatially averaged temperature field, $\tau_E=RC$ is the electrical time constant, and p, A_s, and $\epsilon=\epsilon_0\epsilon_r$ are the pyroelectric coefficient, the area, and the dielectric constant of the pyroelectric sensor, respectively.

In order to find the stationary field $T_p(x,t)$ one must solve the coupled one-dimensional heat-diffusion equations for each layer of the system in Fig. 1:[61]

$$\frac{\partial^2 T_j(x)}{\partial x^2}-\frac{i\omega}{\alpha_j}T_j(x)=\begin{cases}0, & j=g,w,p,s,b \quad (2.2a)\\ \dfrac{H_0\beta\eta_m}{2k_m}\exp[\beta(x+d_1)]+\dfrac{RH_0\beta\eta_m}{2k_m}\exp(-\beta L_m)\exp[-\beta(x+d_2)], & j=m \quad (2.2b)\end{cases}$$

where, for $j=m$, the terms on the right-hand side represent two heat sources in the sample due to the incident and reflected radiation waves, respectively. Here k is the thermal conductivity and $\alpha=k/\rho c$ is the thermal diffusivity with ρ the density and c the specific heat at constant pressure.

The system of Eqs. (2.2) becomes consistent if we consider the following boundary conditions at all interfaces for the temperature continuity,

$$T_i(\text{boundary } i,j)=T_j(\text{boundary } i,j)\ ,(i,j)=(g,w),(w,m),(m,p),(p,s),(s,b) \quad (2.3)$$

and for the heat-flux continuity,

$$k_i\frac{\partial}{\partial x}T_i(\text{boundary } i,j)-k_j\frac{\partial}{\partial x}T_j(\text{boundary } i,j)=\begin{cases}0, & (i,j)=(g,w),\ (w,m),\ (p,s),\ (s,b) \quad (2.4a)\\ (1-R)(H_0/2)\eta_r\exp(-\beta L_m)=G, & (i,j)=(p,m)\ . \quad (2.4b)\end{cases}$$

It can be shown that in Eqs. (2.4) the radiative heat losses are negligible.[60] The third heat source G is developed at the interface m,p and is most conveniently accounted for by the additional heat-flux term in Eq. (2.4).[60] With Eq. (2.1) and using standard algebraic procedures,[20,60] the general expression for the complex PPE voltage response of the system in Fig. 1 is obtained:

$$V(t)=V\Gamma\exp(i\omega t)\ , \quad (2.5)$$

where

$$V=\frac{A\alpha_p\tau_E}{k_p(1+i\omega\tau_E)}\ , \quad (2.6)$$

and the dimensionless factor Γ stands for

$$\begin{aligned}\Gamma=&\exp(-\beta L_m)\{2\eta_m(1-r^{-2})^{-1}[W^r_+\exp(\beta L_m)+RW^r_-\exp(-\beta L_m)]\\ &-[(1-r^{-1})^{-1}\eta_m-R(1+r^{-1})^{-1}\eta_m-(1-R)\eta_r]W_+M\\ &+[(1+r^{-1})^{-1}\eta_m-R(1-r^{-1})^{-1}\eta_m-(1-R)\eta_r]W_-M^{-1}\}[S_+(P-1)+S_-(P^{-1}-1)]\\ &\times\{[(b_{mp}+1)S_+P-(b_{mp}-1)S_-P^{-1}]W_+M+[(b_{mp}-1)S_+P-(b_{mp}+1)S_-P^{-1}]W_-M^{-1}\}^{-1}\ . \quad (2.7)\end{aligned}$$

The following notation was used:

$$\begin{aligned}&W_\pm\equiv\exp(\sigma_wL_w)(b_{gw}+1)(b_{wm}\pm1)+\exp(-\sigma_wL_w)(b_{gw}-1)(b_{wm}\mp1)\ ,\\ &W^r_\pm\equiv\exp(\sigma_wL_w)(b_{gw}+1)(b_{wm}r^{-1}\pm1)+\exp(-\sigma_wL_w)(b_{gw}-1)(b_{wm}r^{-1}\mp1)\ ,\\ &S_\pm\equiv\exp(\sigma_sL_s)(b_{bs}+1)(b_{sp}\pm1)+\exp(-\sigma_sL_s)(b_{bs}-1)(b_{sp}\mp1)\ ,\\ &M\equiv\exp(\sigma_mL_m),\quad P\equiv\exp(\sigma_pL_p),\quad b_{ij}\equiv k_i\sigma_i/k_j\sigma_j,\quad r\equiv\beta/\sigma_m,\quad A\equiv pH_0/2\epsilon\ .\end{aligned} \quad (2.8)$$

Also, $\sigma_j\equiv(1+i)a_j$ is the complex thermal-diffusion coefficient. The reciprocal of its real part,

$$a_j^{-1}\equiv\mu_j\equiv(2\alpha_j/\omega)^{1/2}\ , \quad (2.9)$$

is known as the thermal-diffusion length, by analogy with the optical-absorption length $\mu=\beta^{-1}$. The dimensionless products a_jL_j and βL_m will be referred to as the thermal and optical thicknesses, respectively. The separation in Eq. (2.5) of the time-independent part of the signal into two factors is convenient for the discussion of the special cases in the next section.

III. SPECIAL CASES AND THEIR INTERPRETATION

The discussion hereafter will focus on the amplitude and phase of $V(t)$, Eq. (2.5). The physical quantities contained there in are of two types: a set describing the material properties—η_m,η_r,R,b_{ij}—and a set depending rather on the experimental conditions–$\omega,\beta(\lambda),L_i,r$. Due to the large number of these parameters, for the physical interpretation of the general PPE signal it is desirable to separate the different contributions to the total signal by considering several levels of particularization and by identifying at each level the relevant variables and parameters (Fig. 2).

Concerning the signal-measurement conditions, it should be noted that the current (C) mode, when $\omega\tau_E\ll1$, is more common with the pyroelectric sensors since it assures a flat frequency response, in contrast with the voltage (V) mode, when $\omega\tau_E\gg1$.[62,63] According to Eq. (2.6), the transition between the two modes is simply described by

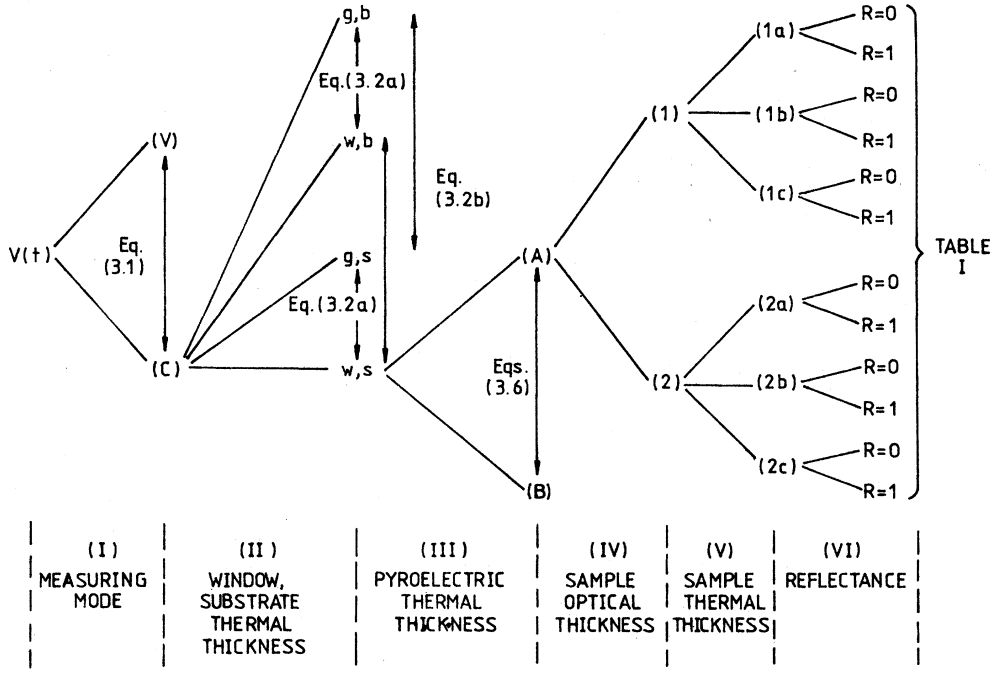

FIG. 2. The levels of particularization of Eq. (2.5). Indicated at each level are the respective special cases and the transition rules between them, as well as the part of the physical system involved.

$$V_C=\frac{A\alpha_p\tau_E}{k_p}\leftrightarrow V_V=V_C\frac{\exp(-i\pi/2)}{\omega\tau_E}\ . \tag{3.1}$$

The following development assumes the C signal-measurement mode.

As a further step, it can be understood intuitively that the qualitative features of the signal do not change to the limit $a_wL_w\gg1$ and $a_sL_s\gg1$, with the advantage of decreasing the number of parameters. In Eqs. (2.8), the last term of $W_\pm, W_\pm^r, S_\pm$ are then vanishing and Γ becomes independent of the gas and backing properties, as expected. For the other limits, from symmetry considerations, the following substitutions of subscripts in $V(t)$ must be carried out:

$$w(a_wL_w\gg1)\leftrightarrow g(a_wL_w\ll1) \tag{3.2a}$$

and/or

$$s(a_sL_s\gg1)\leftrightarrow b(a_sL_s\ll1)\ , \tag{3.2b}$$

indicating that the gas and/or backing have replaced the window and/or substrate.

A third level of particularization (Fig. 2) is to distinguish between two cases.

Case A. Thermally thick pyroelectric ($a_pL_p>1$). Then $P^{-1}\cong0$ and Eq. (2.7) further reduces to

$$\begin{aligned}\Gamma_A=\{&2\eta_m(1-r^{-2})^{-1}[(b_{wm}r^{-1}+1)+R(b_{wm}r^{-1}-1)\exp(-2\beta L_m)]\\&-\exp(-\beta L_m)[(1-r^{-1})^{-1}\eta_m-R(1+r^{-1})^{-1}\eta_m-(1-R)\eta_r](b_{wm}+1)M\\&+\exp(-\beta L_m)[(1+r^{-1})^{-1}\eta_m-R(1-r^{-1})^{-1}\eta_m-(1-R)\eta_r](b_{wm}-1)M^{-1}\}\\&\times[(b_{wm}+1)(b_{mp}+1)M+(b_{wm}-1)(b_{mp}-1)M^{-1}]^{-1}\ .\end{aligned} \tag{3.3}$$

Equation (3.3) is independent of the thermal properties of the substrate because no thermal information reaches it.

Case B. Thermally thin pyroelectric ($a_pL_p<1$). Then $P\cong1+\sigma_pL_p$, $P^{-1}\cong1-\sigma_pL_p$, and by using Eq. (3.3), Eq. (2.7) reduces to the short-form expression

$$\Gamma=\Gamma_A(\text{subscripts } p\rightarrow\text{subscripts } s)\sigma_pL_pb_{ps}\ . \tag{3.4}$$

The following assumption was made in the denominator of Eq. (2.7):

$$a_pL_p(b_{mp}+b_{ps})<(b_{ms}+1)\ , \tag{3.5}$$

which is valid for a sufficiently small value of a_pL_p.

If the factor $\sigma_pL_pb_{ps}$ in Eq. (3.4) is included in the expression for V_{CB}, one finds the rules for the transition be-

tween cases A and B:

$$V_{CA}=V_C\leftrightarrow V_{CB}=Ak_s^{-1}\alpha_s^{1/2}L_p\omega^{1/2}\tau_E\exp(i\pi/4)\ , \quad (3.6a)$$

$$\Gamma_A\leftrightarrow\Gamma_B=\Gamma_A(\text{subscripts } p\rightarrow\text{subscripts } s)\ , \quad (3.6b)$$

indicating the obvious result that the substrate has now replaced the pyroelectric because the thermal wave is transferred practically unaffected from the sample to the substrate.

The directly accessible experimental variables are the modulation angular frequency of the radiation, ω, and its wavelength λ, which are related to a_j and β, respectively. Following the similar schemes of Refs. 1, 20, and 64, the criteria for further particularizations are the thermal and optical thicknesses a_mL_m and βL_m of the sample. The only factor in Eq. (2.5) concerned is Γ_A, Eq. (3.3). The six possible subcases of case A are shown schematically in Fig. 3. The sample and the pyroelectric are drawn apart in order to allow for the representation of the characteristic lengths μ_m and μ that exceed the sample thickness L_m. For the first group (1) the sample is optically thick and for the second group (2) it is optically thin. All inequalities are assumed to be fulfilled by several orders of magnitude and the pyroelectric is considered thermally thick (case A).

Case (1a). Optically thick and thermally thin sample ($a_mL_m<1<\beta L_m$, $|r^{-1}|\ll 1$). In Eq. (3.3) set $\exp(-\beta L_m)\cong 0$ and $\exp(\pm\sigma_mL_m)\cong 1$. One obtains

$$\Gamma_A=\frac{\eta_m}{b_{wp}+1}\ . \quad (3.7)$$

The signal is saturated with respect to β and a_m and is independent of the reflectance R since the whole radiation is adsorbed within the sample. The signal reaches the pyroelectric via unattenuated thermal transmission.

Case (1b). Optically and thermally thick sample ($1<a_mL_m<\beta L_m$, $|r^{-1}|<1$). Then $\exp(-\beta L_m)<|\exp(-\sigma_mL_m)|\cong 0$, and keeping in Γ_A only the largest term, one obtains

$$\Gamma_A=\frac{2\eta_m}{(b_{mp}+1)(b_{wm}+1)}\exp[-(1+i)a_mL_m]\ . \quad (3.8)$$

The signal depends strongly on the product a_mL_m. It reaches the pyroelectric as an exponentially attenuated thermal transmission wave and is independent of R, as in case (1a). The phase lag increases linearly with a_mL_m, and is thus unstable with the frequency.

Case 1(c). Optically and thermally thick sample ($1<\beta L_m<a_mL_m$, $|r^{-1}|>1$). Then $|\exp(-\sigma_mL_m)|<\exp(-\beta L_m)\cong 0$, and keeping in Γ_A only the largest term, one obtains this time

$$\Gamma_A=\frac{(1-R)\eta_r+(1+R)\eta_m r}{b_{mp}+1}\exp(-\beta L_m)\ , \quad (3.9)$$

which yields for $R=0$ and $\eta_r=\eta_m$

$$\Gamma_A=\frac{\eta_r(1-R)(1-\beta L_m)+\eta_m[(1+R)\beta L_m+(1-R)r^{-2}]}{b_{wp}+1}\ . \quad (3.12)$$

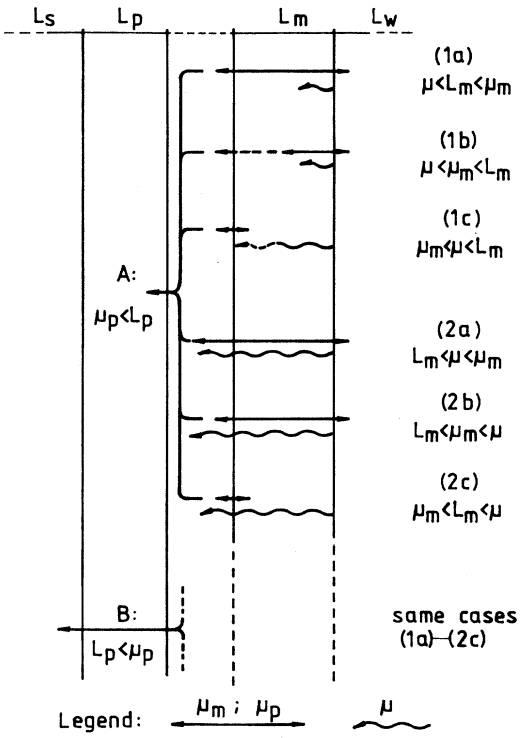

FIG. 3. Various possible special cases of the PPE response, depending on the relative magnitude of the sample thermal diffusion length μ_m, sample optical-absorption length μ, and sample thickness L_m. The group of cases A and B apply for a thermally thick and thin pyroelectric, respectively.

$$\Gamma_A=\frac{\eta_r}{b_{mp}+1}\exp(-\beta L_m)\ , \quad (3.10)$$

while, for $R=1$,

$$\Gamma_A=\frac{\eta_m\beta(2/\sqrt{2}a_m)}{b_{mp}+1}\exp(-\beta L_m)\exp(-i\pi/4)\ . \quad (3.11)$$

Figure 3 suggests that case (1c) is basically an optical transmission spectroscopy case. For $R=0$ [Eq. (3.10)], the exponential tail of the transmitted light produces the signal directly via absorption in the reflector. For $R=1$ [Eq. (3.11)], the exponential tail of the transmitted light is reflected back. Only the heat generated by the fraction absorbed upon the double path in the sample layer close to the pyroelectric, of an effective thickness $\mu_m/\sqrt{2}$, is communicated to the sensor. Equation (3.11) thus describes a combined optical transmission-absorption spectroscopy with path lengths L_m and $2(\mu_m/\sqrt{2})$, respectively. The phase lag increases with R from 0 to $\pi/4$.

Case (2a). Optically and thermally thin sample ($a_mL_m<\beta L_m<1$, $|r^{-1}|<1$). In Eq. (3.3) set $\exp(-\beta L_m)\cong 1-\beta L_m$ and $\exp(\pm\sigma_mL_m)\cong 1$. After some algebraic manipulations, the result takes the form

Case 2(b). Optically and thermally thin sample ($\beta L_m < a_m L_m < 1$, $|r^{-1}| > 1$). With the same values of the exponentials as is case (2a), the result is similar to Eq. (3.12), implying that to a first approximation cases (2a) and (2b) are equivalent:

$$\Gamma_A = \frac{\eta_r(1-R)(1-\beta L_m)+\eta_m[(1+R)\beta L_m-(1-R)r^2]}{b_{wp}+1} . \tag{3.13}$$

Indeed, for $R=0$, Eqs. (3.12) and (3.13) can be approximated by

$$\Gamma_A = \frac{\eta_r+(\eta_m-\eta_r)\beta L_m}{b_{wp}+1} \cong \frac{\eta_r}{b_{wp}+1} . \tag{3.14}$$

The sample is practically transparent and the radiation is absorbed mainly in the reflector. The essentially saturated signal still contains a weak dependence on r^{-2} [case (2a)] or r^2 [case (2b)]. These are purely imaginary quantities and can be recovered from the signal by quadrature lock-in detection.

The situation $R=1$ justifies the presence of the higher term in the series expansion of $\exp(-\beta L_m)$, when both Eqs. (3.12) and (3.13) reduce to

$$\Gamma_A = \frac{\eta_m \beta(2L_m)}{b_{wp}+1} . \tag{3.15}$$

All the radiation is reflected back, so that the signal is due to the small fraction absorbed upon the double path $2L_m$ in the sample. The heat is communicated unattenuated to the sensor and it results in an optical-absorption-spectroscopy case.

Case (2c). Optically thin and thermally thick sample ($\beta L_m < 1 < a_m L_m$, $|r^{-1}| \gg 1$). The approximations in Eq. (3.3) are $\exp(-\beta L_m) \cong 1$ and, $\exp(-\sigma_m L_m) \cong 0$, and the result is

$$\Gamma_A = \frac{(1-R)\eta_r+(1+R)\eta_m r}{b_{mp}+1} , \tag{3.16}$$

which, for $R=0$, yields

$$\Gamma_A = \frac{\eta_r}{b_{mp}+1} , \tag{3.17}$$

describing a saturated signal, generated by direct absorption in the reflector, whereas, for $R=1$,

$$\Gamma_A = \frac{\eta_m \beta(2/\sqrt{2}a_m)}{b_{mp}+1}\exp(-i\pi/4) . \tag{3.18}$$

Now the transmitted signal is reflected back and only the heat generated by the fraction absorbed upon double path in the sample layer close to the pyroelectric, of an effective thickness $\mu_m/\sqrt{2}$, is communicated to the sensor, Fig. 3. Therefore, Eq. (3.18) describes an optical-absorption-spectroscopy case with path length $2(\mu_m/\sqrt{2})$. The phase lag increases with R from 0 to $\pi/4$, but, in contrast to case (1c), the transmitted radiation here is practically unattenuated.

IV. DISCUSSION AND NUMERICAL EVALUATIONS

In standard spectrophotometers, the sample and the detector are apart from one another and the measurements produce transmission spectra. The consequence of the intimate contact between the sensor and the sample in the PPE method is the existence of two channels for the transfer of information from the sample to the sensor: the thermal channel, consisting of radiation absorption within the sample and transmission of this information via thermal waves to the sensor, and the optical channel, consisting of penetration of the radiation through the sample and absorption of the transmitted fraction in the detector. This statement is expressed quantitatively in Table I, summarizing the special cases (1a)–(1c) and (2a)–(2c).

There are three basic response types, mediated, respectively, by (i) the thermal channel, (ii) the optical channel, and (iii) the thermal and optical channel. Some factors are rewritten in an exponential form, allowing for a better correlation with the physical phenomena depicted in Fig. 3. The relative contribution of the two signal com-

TABLE I. The particular expressions for the factor Γ_A, rewritten in exponential form and grouped according to the specific coupling channel between the sample and the pyroelectric. Two extreme values for the reflectance are considered.

Coupling channel	Special cases	$R=0$ $\lvert\Gamma_A\rvert$	$R=0$ Phase (rad)	$R=1$ $\lvert\Gamma_A\rvert$	$R=1$ Phase (rad)
(i) thermal	(1a)	$\frac{\eta_m \exp(-a_m L_m)}{b_{wp}+1}$	$-a_m L_m$	$\frac{\eta_m \exp(-a_m L_m)}{b_{wp}+1}$	$-a_m L_m$
	(1b)	$\frac{2\eta_m \exp(-a_m L_m)}{(b_{mp}+1)(b_{wm}+1)}$		$\frac{2\eta_m \exp(-a_m L_m)}{(b_{mp}+1)(b_{wm}+1)}$	
(ii) optical	(1c)	$\frac{\eta_r \exp(-\beta L_m)}{b_{mp}+1}$	0	$\frac{\eta_m \exp(-\beta L_m)\{1-\exp[-\beta(2\mu_m/\sqrt{2})]\}}{b_{mp}+1}$	$-\pi/4$
	(2c)				
(iii) thermal, optical	(2a)	$\frac{\eta_r}{b_{wp}+1}$	0	$\frac{\eta_m[1-\exp(-2\beta L_m)]}{b_{wp}+1}$	0
	(2b)				

ponents is dictated, among other parameters, by the reflectance R, resulting in optical-transmission- or optical-absorption-spectroscopic capabilities of the PPE method, for $R=0$ or $R=1$, respectively.

We shall examine some experimental situations that cannot be explained without considering a finite reflectance $R\neq 0$, but first it should be mentioned that, for $R=0$, $\omega\tau_E \gg 1$ and $a_w L_w = a_s L_s = 0$, our Eq. (2.5) is similar to Eq. (23) in Ref. 20, for $\beta_p L_p$ and $|r_p| \gg 1$, as expected. The normalized signal in the reflection-mode PPE spectroscopy,[40] Eqs. (4)–(6) in Ref. 59, corresponds to cases (i)–(iii) in Table I. Also, the overall signal [Eq. (3) of Ref. 59] can be obtained from Eq. (3.3), provided that $b_{mp}=b_{wm}=1$ and $\eta_r=\eta_m=1$. Investigations on thermally and optically thin samples with a transparent and thermally thin pyroelectric sensor[65] should be assigned to case B(iii) ($R=1$), but only with a single path length L_m:

$$V \sim \eta_m [1-\exp(-\beta L_m)] \ . \tag{4.1}$$

The experiments of Refs. 32 and 66 can be viewed as a superposition of cases (1b) and (2c). A signal is generated in the sample by the irradiation fraction $2H_0\beta_1 L_1$ and another one is generated in the reflector, i.e., reference sample, by the fraction $H_0(1-\beta_1 L_1)$. Their sum, Eqs. (3.8) and (3.16),

$$V \sim 4\eta_m \beta_1 L_1 \exp[-(1+i)a_2 L_2] + \eta_r (1-R)(1-\beta_1 L_1) \ , \tag{4.2}$$

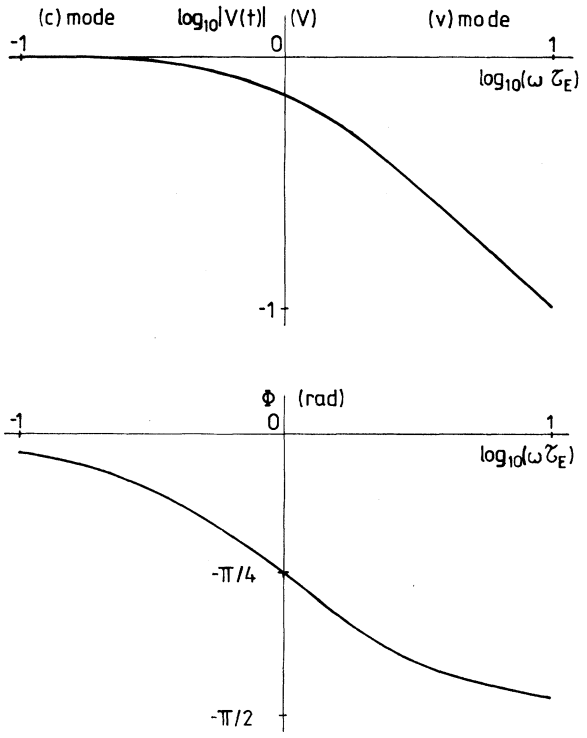

FIG. 4. Normalized PPE signal amplitude and phase vs normalized frequency, for $\Gamma=1$, modeled by the transfer function of a low-pass RC quadrupole, showing the transition between the current - (C) and voltage- (V) measurement modes.

is analogous with Eq. (6a) in Ref. 32 and Eq. (2) in Ref. 66.

An alternative way of looking into the physics of the PPE method is to perform numerical simulations and to assign the analytic expressions for the special cases to well-defined regions. The interpretation of the first two particularization levels (Fig. 2) is straightforward. The transition from the C to the V [Eq. (3.1)] mode at the transition frequency $\omega_{VC}=\tau_E^{-1}$ is represented in Fig. 4. Equations (3.2a) and (3.2b) also imply two frequency-dependent transitions centered at $a_w L_w=1$ and $a_s L_s=1$. All the following representations assume C-mode signal acquisition from a PPE system with $V_C=1V$, $\eta_r=\eta_m=1$, and $a_w L_w = a_s L_s = 10^{15}\omega^{1/2} \gg 1$.

Cases A and B differ mainly by the factors V_{CA} and V_{CB}, Eq. (3.6). In Fig. 5 the calculated signal amplitude and phase when Eq. (3.5) holds true, curve (a), and in the two other situations when Eq. (3.5) is not satisfied, curves (b) and (c), show that far from the B-A boundary the signal behaves according to Eq. (3.6a).

The variation of the factor Γ_A alone can be studied when the conditions are set for sweeping the six cases (1a)–(1c) and (2a)–(2c) and for settling case A throughout the entire frequency range of interest. The special cases depend on two independent material parameters, b_{wm} and b_{mp}. The maximum value $\Gamma_A=1$ is obtained in Figs.

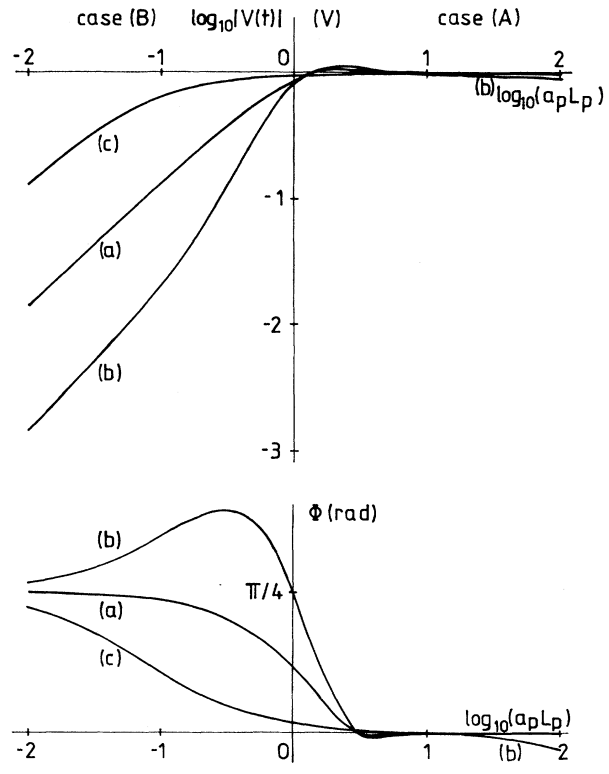

FIG. 5. PPE signal amplitude and phase in case (1a) vs thermal thickness of the pyroelectric, showing the transition between the thermally thin (B) and thick (A) cases, in three situations: (a) $b_{mp}=1$; (b) $b_{mp}=10$; (c) $b_{mp}=10^{-1}$. For all curves, $b_{wm}=10^{-5}$, $b_{sm}=1$, $(2\alpha_p)^{-1/2}L_p=1\ \mathrm{s}^{1/2}$. Case (1a) is defined by $(2\alpha_m)^{-1/2}L_m=10^{-4}\ \mathrm{s}^{1/2}$, $\omega=10^{-6}$–$10^{4}\ \mathrm{rad\,s}^{-1}$, and $\beta L_m=10^4$.

6(a) and 6(b). It clearly results that, for $R=0$, the signal is not saturated only in two regions, (1b) and (1c), allowing for thermal or optical investigations of material properties. On the other hand, for $R=1$, the general remark is that the signal contains more information about the sample. Regions (1a) and (1b) remain unchanged, but in the regions (2a), (2b), and (2c) the signal increases with increasing β, yielding an absorption spectrum. In region (1c), it still decreases sharply with increasing β, as for $R=0$, yielding the same transmission spectrum (see, for comparison, Table I). The transition between the two β dependencies due to changes of experimental conditions gives rise to spectral inversions via two different mechanisms,[59] but only for $R\neq 0$. Figures 8(b) and 8(d) explain such experimentally observed inversions, which were produced by changing the thermal thickness of the sample,[18] or both its thermal and optical thickness.[40] Besides the β dependence, region (2c) has a negative slope with respect to $a_m L_m$.

The contributions of the factor Γ_A to the PPE signal phase lag with respect to the modulation, are presented in Figs. 6(c) and 6(d). In region (1b) the phase lag increases progressively with $a_m L_m$ and then it recovers very sharply to the initial value at the (1b)-(1c) boundary. This feature suggests that one use, experimentally, the phase rather than the amplitude of the signal as a sensitive means of measuring small changes of the variables, when $a_m L_m \cong \beta L_m$.

The amplitude and phase surfaces for the other three possible combinations of b_{wm} and b_{mp} values, compared to unity, are displayed in Figs. 7–9. A comparative inspection of Figs. 7(a) and 7(b), 8(a) and 8(b), and 9(a) and 9(b) reveals that, to the limit of the thermally very thin sample ($a_m L_m \ll 1$), the signal amplitude depends only on b_{wp}, whereas to the limit of the thermally very thick sample ($a_m L_m \gg 1$) it depends only on b_{mp}, in agreement with Table I. Since the amplitude surfaces at these two far ends has different heights, in the (a)–(c) transition zone new ω and β dependencies are found. Furthermore, the transition zones are particularly interesting for experimental investigations due to the fact that, under proper conditions, the signal here is proportional to the sample specific heat c^{-1} [see location of experiment[56] in Figs. 8(a) and 8(c)], or to the thermal conductivity $k_m^{\pm 1}$ alone. All these phenomena taking place in the transition zones are reflected in the phase surfaces as a decrease [Figs. 7(c) and 7(d)] or an increase [Figs. 8(c) and 8(d)] of the phase lag as compared to Figs. 6(c) and 6(d).

Figures 4–9 are the graphic equivalent of Eqs. (3.1), (3.6), and Table I, allowing for the graphic construction of the PPE signal surfaces, for any experimental configurations. The method proceeds as follows: the first step is to construct a coordinate system analogous to the one in Fig. 10, with the correct location of the transition points on the ω axis depending on the PPE cell structure chosen. Then one combines the appropriate representations, by algebraically adding the phases and the amplitude logarithms point by point. Unlike the analytic construction procedure given in Sec. III, the graphic method is also valid in the transition zones and offers a synthetic overview of all subcases simultaneously.

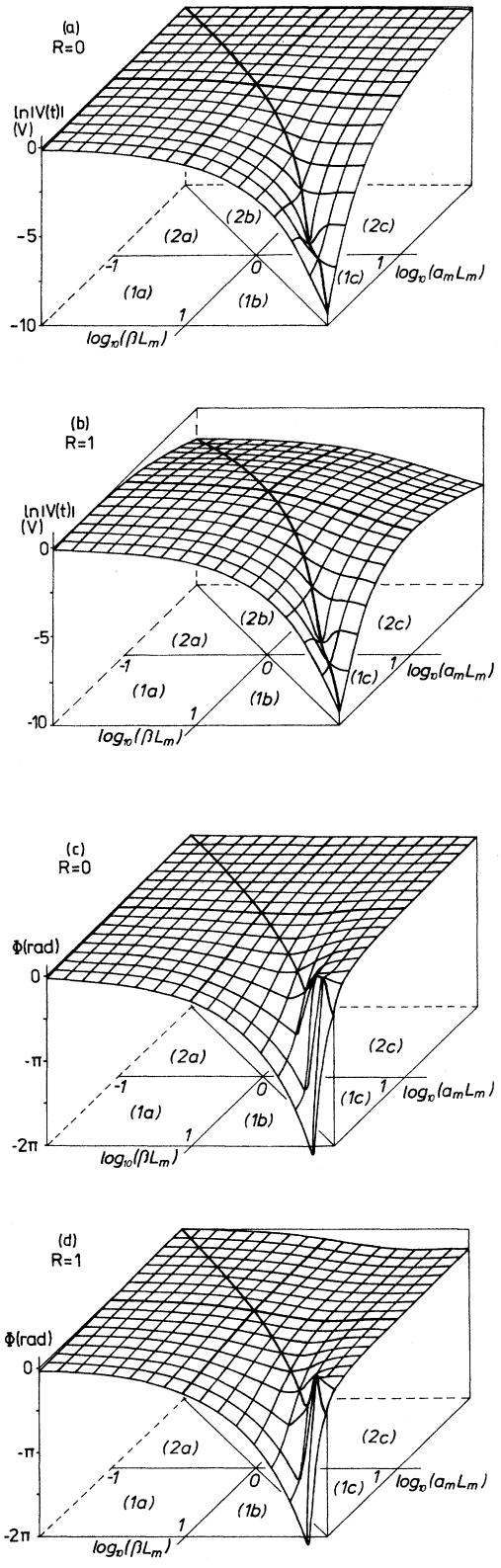

FIG. 6. PPE signal amplitude [panels (a) and (b)] and phase [panels (c) and (d)] surfaces vs sample thermal and optical thickness, for two extreme values of the reflectance $R=0$ and $R=1$. The relevant material parameters are $(2\alpha_p)^{-1/2}L_p=10^7$ s$^{1/2}$, $(2\alpha_m)^{-1/2}L_m=10^{-1}$ s$^{1/2}$, $b_{wm}=1$, and $b_{mp}=10^{-4}$.

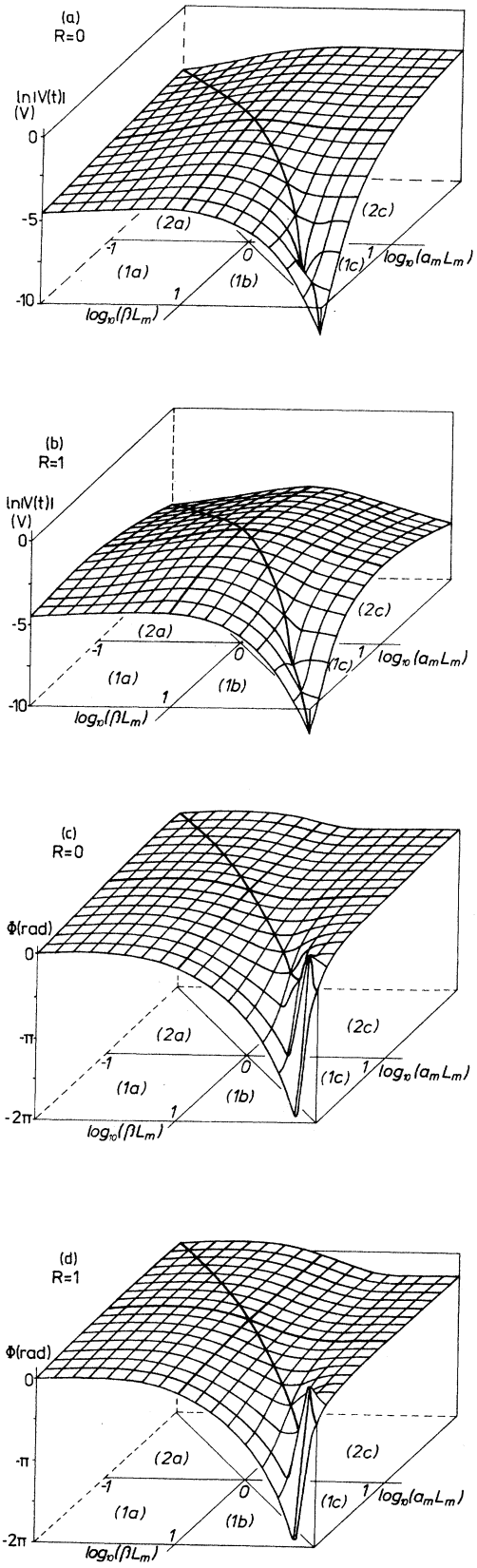

FIG. 7. Same as in Fig. 6, but $b_{wm}=10$ and $b_{mp}=10$.

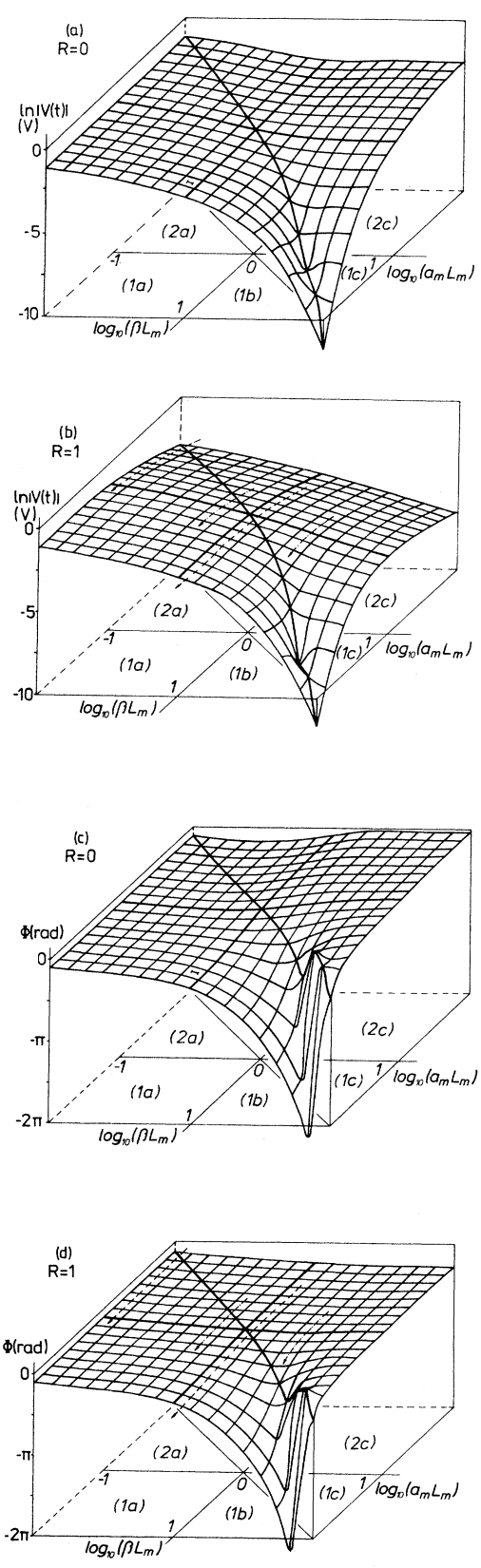

FIG. 8. Same as in Fig. 6, but $b_{wm}=10^{-1}$ and $b_{mp}=10$. The location of the experiments of Ref. 56 (⟼), Ref. 40 (– – – →), and Ref. 18 (– · – · →), is also shown.

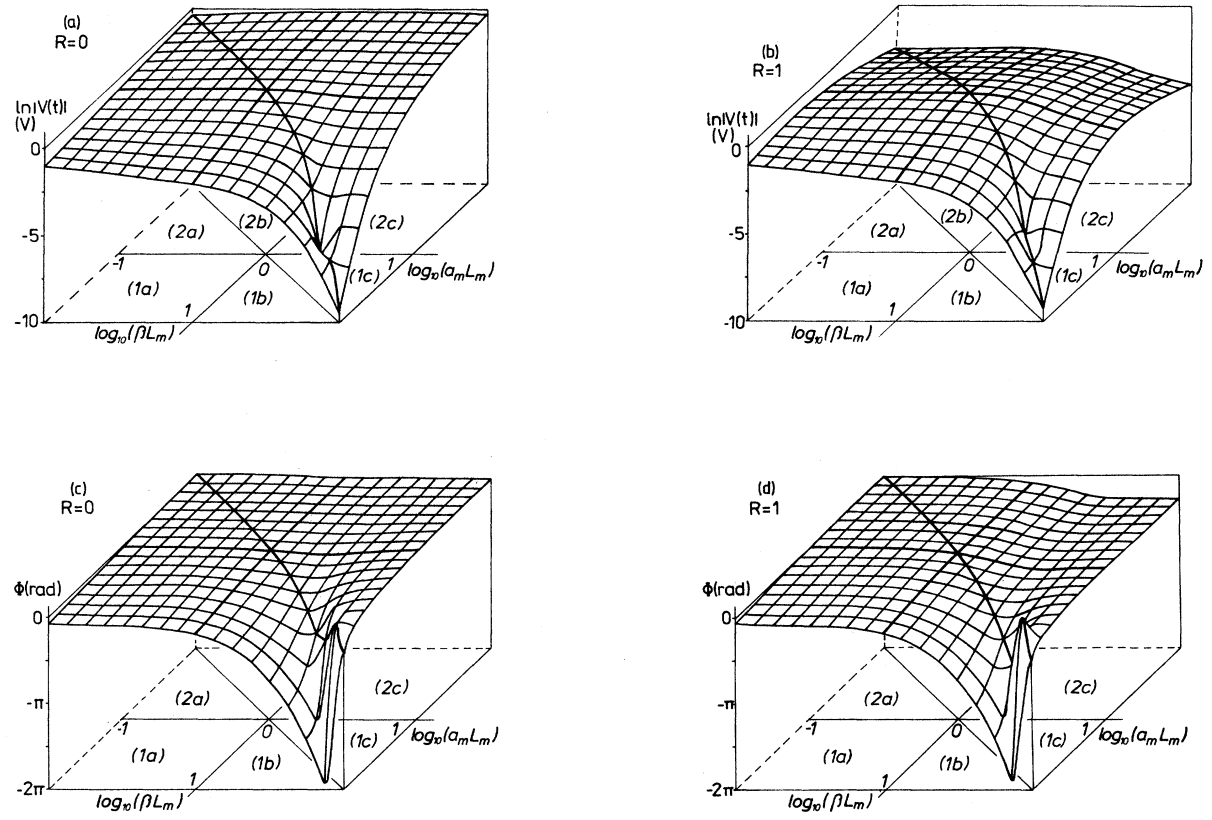

FIG. 9. Same as in Fig. 6, but $b_{wm}=10$ and $b_{mp}=10^{-1}$.

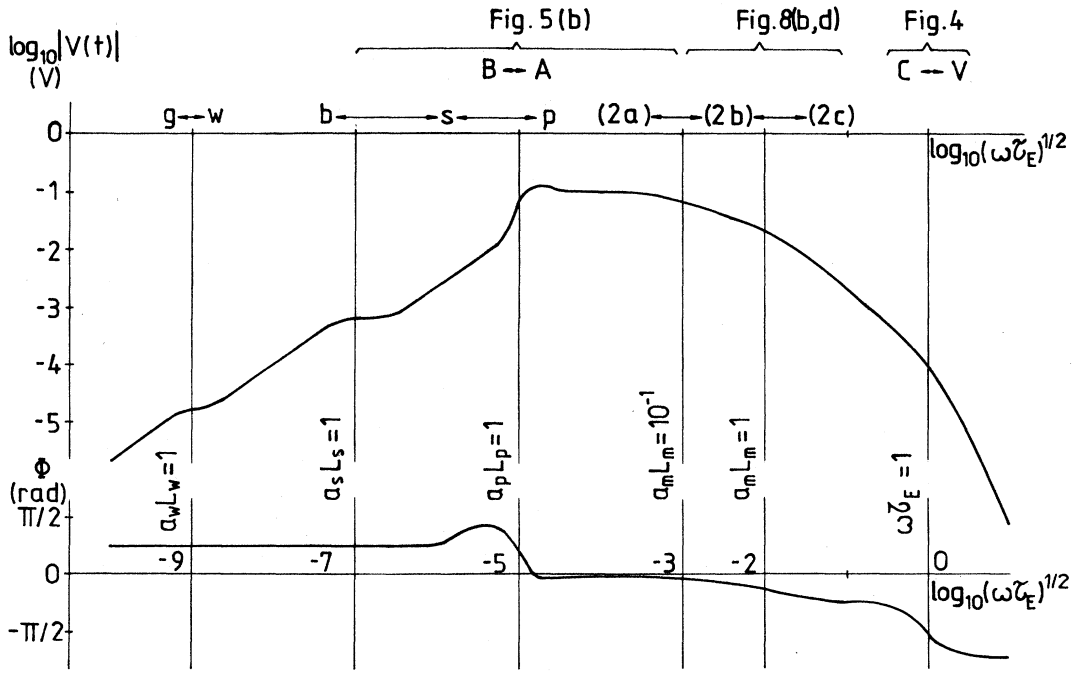

FIG. 10. Example for the graphic construction method of the overall PPE signal amplitude and phase, using Figs. 4–9. The parameters are $R=1$, $\beta L_m=10^{-1}$, $b_{gw}=10^{-3}$, $b_{wm}=10^{-1}$, $b_{mp}=10$, $b_{ps}=10^{-1}$, and $b_{sb}=10$. The values for other parameters result from the position of the characteristic points on the frequency axis.

V. CONCLUSIONS

A theory for the voltage response of a six-layer photopyroelectric cell with periodic excitation was developed which takes into consideration a voltage- or current-measurement mode and a finite reflectance at the sample-pyroelectric interface. It is shown that the assumption of an arbitrary value for the reflectance completely changes the physical picture of the PPE effect, featuring simultaneous optical-absorption and -transmission characteristics and creating very diverse experimental opportunities for optical and thermal investigations of solid, liquid, or even gaseous substances. At the same time, the coexistence of these two complementary processes produces unusual effects, such as the experimentally observed spectral peak inversions and distortions, or the local amplitude wells and steep phase changes, predicted theoretically in Sec. IV. Additional difficulties in the interpretation of the PPE signals may arise from the wavelength-dependent surface absorptance and reflectance of the sample, resulting in absorptionlike spectra, even in the saturated cases. Also, the contribution of the photoacoustic response should be taken into consideration, especially when the PPE signal is strongly damped.

The cell geometry of Fig. 1 fits, after suitable particularizations, most of the reported PPE experiments. However, other configurations might be more advantageous in some cases, e.g., with a lateral irradiation.[35] The theory presented in Ref. 20 is a particular case of the present theory since it assumes total radiation absorption and a voltage-mode signal measurement. In these conditions, the two approaches yield essentially the same results, with the exception of case (1c), where a significant term was neglected during a different approximation procedure used in that reference.[67]

The PPE response for any special case out of the 194 possible combinations, can be derived by using Table I and the transition rules from Sec. III. A graphic method for the construction of a particular PPE response is also given. Both methods are proved to be useful tools for a systematic interpretation and evaluation of recent PPE experiments involving material characterization.

It is our belief that the full potentiality of the PPE technique for optical and thermal material properties investigation remains to be demonstrated by future experiments, in parallel and in competition with the PPE technique with pulsed excitation sources.

ACKNOWLEDGMENTS

The authors are grateful to Ileana Chirtoc and Judith Szentgyörgyi for their contribution to this work.

[1]A. C. Tam, Rev. Mod. Phys. **58**, 381 (1986).
[2]A. Rosencwaig, *Photoacoustics and Photoacoustic Spectroscopy* (Wiley, New York, 1980).
[3]C. K. N. Patel and A. C. Tam, Rev. Mod. Phys. **53**, 517 (1981).
[4]*Photoacoustic and Photothermal Phenomena,* edited by P. Hess and J. Pelzl (Springer, Heidelberg, 1988).
[5]W. J. Parker, R. J. Jenkins, C. P. Butler, and G. L. Abbott, J. Appl. Phys. **32**, 1679 (1961).
[6]K. Tanaka, R. Satch, and A. Odajima, Jpn. J. Appl. Phys. **22**, L592 (1983).
[7]J. H. Jacob, E. R. Pugh, J. D. Daugherty, and D. B. Northam, Rev. Sci. Instrum. **44**, 471 (1973).
[8]G. H. Brilmyer, A. Fujishima, K. S. V. Santhanam, and A. J. Bard, Anal. Chem. **49**, 2057 (1977).
[9]M. Bass, E. W. Van Stryland, and A. F. Steward, Appl. Phys. Lett. **34**, 142 (1979).
[10]M. Bass and L. Liou, J. Appl. Phys. **56**, 184 (1984).
[11]G. Gafni, A. Eliahu, and H. Galron, Rev. Sci. Instrum. **58**, 357 (1987).
[12]S. B. Lang, *Sourcebook of Pyroelectricity* (Gordon and Breach, London, 1974).
[13]S. B. Lang, *Literature Guide to Pyroelectricity,* appearing periodically, beginning with Ferroelectrics **5**, 125 (1973).
[14]Y. Ta, C.R. Acad. Sci. Paris **207**, 1042 (1938).
[15]J. Cooper, Rev. Sci. Instrum. **33**, 92 (1962).
[16]S. B. Lang and F. Steckel, Rev. Sci. Instrum. **36**, 1817 (1965).
[17]H. Coufal, Appl. Phys. Lett. **44**, 59 (1984).
[18]A. Mandelis, Chem. Phys. Lett. **108**, 388 (1984).
[19]D. Dădârlat, M. Chirtoc, R. M. Cândea, and I. Bratu, Infrared Phys. **24**, 469 (1984).
[20]A. Mandelis and M. M. Zver, J. Appl. Phys. **57**, 4421 (1985).
[21]R. Peterson, G. Day, P. Gruzensky, and R. Phelan, J. Appl. Phys. **45**, 3296 (1974).
[22]W. R. Blevin and J. Geist, Appl. Opt. **13**, 1171 (1974).
[23]S. B. Lang, Ferroelectrics **11**, 315 (1976).
[24]C. Jeack, R. Melcher, and S. Jha, J. Appl. Phys. **53**, 3947 (1982).
[25]R. J. Batt, Ferroelectrics **34**, 265 (1981).
[26]A. Van der Ziel and S. Liu, J. Appl. Phys. **43**, 4260 (1972).
[27]A. Van der Ziel, J. Appl. Phys. **44**, 546 (1973).
[28]S. T. Liu and D. Long, Proc. IEEE **66**, 14 (1978).
[29]L. S. Chun, Chin. J. Infrared Millimeter Waves A **6**, 95 (1987).
[30]H. Coufal, Fresenius Z. Anal. Chem. **324**, 456 (1986).
[31]H. Coufal, IEEE Trans. Ultrason. Ferroelec. Freq. Control **UFFC-33**, 507 (1986).
[32]H. Coufal, Appl. Phys. Lett. **45**, 516 (1984).
[33]H. Coufal, R. Grygier, D. Horne, and J. Fromm, J. Vac. Sci. Technol. A **5**, 2875 (1987).
[34]H. Coufal, J. Stöhr, and K. Baberschke, in Ref. 4, p. 25.
[35]T. Hinoue, S. Kawada, M. Murata, and Y. Yokoyama, Chem. Lett. Jpn. 2061 (1988).
[36]*Photoacoustic and Thermal Wave Phenomena in Semiconductors,* edited by A. Mandelis (Elsevier, New York, 1987).
[37]R. K. Grygier, W. Knoll, and H. Coufal, Can. J. Phys. **64**, 1067 (1986).
[38]T. J. Chuang, H. Coufal, and F. Träger, J. Vac. Sci. Technol. A **1**, 236 (1983).
[39]M. Chirtoc, D. Dădârlat, I. Chirtoc, and D. Bicanic, in Ref. 4, p. 55.
[40]M. Chirtoc, D. Dădârlat, I. Chirtoc, and D. Bicanic, Spectrosc. Lett. **21**, 413 (1988).
[41]H. Coufal, H. F. Winters, and F. Sequeda, in Ref. 4, p. 201.
[42]W. Knoll and H. Coufal, in Ref. 4, p. 209.
[43]T. Baumann, Appl. Phys. Lett. **43**, 71 (1983).

[44]I. F. Faria, J. C. Ghizoni, and L. C. Miranda, Appl. Phys. Lett. **47**, 1154 (1985).
[45]M. Liezers and R. M. Miller, in Ref. 4, p. 437.
[46]M. Byfuss, R. Tilgner, and J. Baumann, in Ref. 4, p. 392.
[47]M. V. Iravani and H. K. Wickramasinghe, J. Appl. Phys. **58**, 122 (1985).
[48]M. V. Iravani and M. Nikoonahad, J. Appl. Phys. **62**, 4065 (1987).
[49]T. J. Negran, Ferroelectrics **34**, 285 (1981).
[50]H. Coufal and P. Hefferle, Appl. Phys. A **38**, 213 (1985).
[51]C. C. Ghizoni and L. C. Miranda, Phys. Rev. B **32**, 8392 (1985).
[52]P. K. John, L. C. Miranda, and A. C. Rastogi, Phys. Rev. B **34**, 4342 (1986).
[53]H. Coufal and P. Hefferle, Canad. J. Phys. **64**, 1200 (1986).
[54]M. Liezers and R. M. Miller, in Ref. 4, p. 344.
[55]H. Coufal and W. Lee, Appl. Phys. B **44**, 141 (1987).
[56]A. Mandelis, F. Care, K. K. Chan, and L. C. M. Miranda, Appl. Phys. A **38**, 117 (1985).
[57]J. F. Power and A. Mandelis, Rev. Sci. Instrum. **58**, 2024 (1987).
[58]J. F. Power and A. Mandelis, Rev. Sci. Instrum. **58**, 2033 (1987).
[59]M. Chirtoc and I. Chirtoc, Infrared Phys. **29**, 847 (1989).
[60]R. M. Logan and Katharine Moore, Infrared Phys. **13**, 37 (1973).
[61]H. S. Carslaw and J. C. Jaeger, *Conduction of Heat in Solids*, 2nd ed. (Oxford University Press, London, 1959).
[62]M. Chirtoc, R. M. Cândea, and V. Mercea, Ferroelectrics **56**, 283 (1984).
[63]M. Chirtoc and R. M. Cândea, Rev. Roum. Phys. **31**, 945 (1986).
[64]A. Rosencwaig and A. Gersho, J. Appl. Phys. **47**, 64 (1976).
[65]K. Tanaka, Y. Ichimura, and K. Sindoh, J. Appl. Phys. **63**, 1815 (1988).
[66]A. Mandelis, R. E. Wagner, K. Ghandi, R. Baltman, and Phat Dao, Phys. Rev. B **39**, 5254 (1989).
[67]M. Chirtoc and G. Mihăilescu, Rev. Roum. Phys. (to be published) (Comments on Ref. 20).